The Astrophysical Journal, 702:1005–1015, 2009 September 10 doi:10.1088/0004-637X/702/2/1005

GALAXY MERGERS AND DARK MATTER HALO MERGERS IN ΛCDM: MASS, REDSHIFT, AND MASS-RATIO DEPENDENCE

Kyle R. Stewart[1], James S. Bullock[1], Elizabeth J. Barton[1], and Risa H. Wechsler[2]
[1] Center for Cosmology, Department of Physics and Astronomy, The University of California at Irvine, Irvine, CA 92697, USA
[2] Kavli Institute for Particle Astrophysics & Cosmology, Department of Physics, and SLAC National Accelerator Laboratory, Stanford University, Stanford, CA 94305, USA
Received 2008 November 13; accepted 2009 July 13; published 2009 August 18

ABSTRACT

We employ a high-resolution ΛCDM *N*-body simulation to present merger rate predictions for dark matter (DM) halos and investigate how common merger-related observables for galaxies—such as close pair counts, starburst counts, and the morphologically disturbed fraction—likely scale with luminosity, stellar mass, merger mass ratio, and redshift from $z = 0$ to $z = 4$. We investigate both rate at which subhalos first enter the virial radius of a larger halo (the "infall rate"), and the rate at which subhalos become destroyed, losing 90% of the mass they had at infall (the "destruction rate"). For both merger rate definitions, we provide a simple "universal" fitting formula that describes our derived merger rates for DM halos a function of dark halo mass, merger mass ratio, and redshift, and go on to predict galaxy merger rates using number density matching to associate halos with galaxies. For example, we find that the instantaneous (destruction) merger rate of $m/M > 0.3$ mass-ratio events into typical $L \gtrsim f\ L_*$ galaxies follows the simple relation $dN/dt \simeq 0.03(1 + f)\ \mathrm{Gyr}^{-1}\ (1 + z)^{2.1}$. Despite the rapid increase in merger rate with redshift, only a small fraction of >0.4 L_* high-redshift galaxies (∼3% at $z = 2$) should have experienced a major merger ($m/M > 0.3$) in the very recent past ($t < 100$ Myr). This suggests that short-lived, merger-induced bursts of star formation should not contribute significantly to the global star formation rate at early times, in agreement with several observational indications. In contrast, a fairly high fraction (∼20%) of those $z = 2$ galaxies should have experienced a morphologically transformative merger within a virial dynamical time (∼500 Myr at $z = 2$). We compare our results to observational merger rate estimates from both morphological indicators and pair-fraction-based determinations between $z = 0$ and 2 and show that they are consistent with our predictions. However, we emphasize that great care must be made in these comparisons because the predicted observables depend very sensitively on galaxy luminosity, redshift, overall mass ratio, and uncertain relaxation timescales for merger remnants. We show that the *majority* of bright galaxies at $z = 3$ should have undergone a major merger (>0.3) in the previous 700 Myr and conclude that mergers almost certainly play an important role in delivering baryons and influencing the kinematic properties of Lyman break galaxies (LBGs).

Key words: cosmology: theory – dark matter – galaxies: formation – galaxies: halos – methods: *N*-body simulations

Online-only material: color figures

1. INTRODUCTION

In the current theory of hierarchical structure formation (ΛCDM), dark matter (DM) halos and the galaxies within them are assembled from the continuous accretion of smaller objects (Peebles 1982; Blumenthal et al. 1984; Davis et al. 1985; Wechsler et al. 2002; Fakhouri & Ma 2008; Stewart et al. 2008; Cole et al. 2008; Neistein & Dekel 2008; Wetzel et al. 2009). It is well established that galaxy and halo mergers should be more common at high redshift (e.g., Governato et al. 1999; Carlberg et al. 2000; Gottlöber et al. 2001; Patton et al. 2002; Berrier et al. 2006; Lin et al. 2008; Wetzel et al. 2009), but the precise evolution is expected to depend on details of the mergers considered. Moreover, it is unclear how these mergers manifest themselves in the observed properties of high-z galaxies and what role they play in setting the properties of galaxies in the local universe. Interestingly, there are indications that the familiar bimodality of galaxies as disks versus spheroids at $z = 0$ might be replaced by a categorization of disk-like versus merger-like at higher redshift (Förster Schreiber et al. 2006; Genzel et al. 2006; Law et al. 2007a; Kriek et al. 2008; Melbourne et al. 2008; Shapiro et al. 2008; Wright et al. 2009), although this shift in the dichotomy of galaxy morphologies is by no means robust and requires further study. In this paper, we use *N*-body simulations to provide robust predictions and simple fitting functions for DM halo merger rates and merger fractions as a function of redshift, mass, and mass ratio. We use our predictions to address two observable consequences of galaxy mergers—merger-driven starbursts and morphological disturbances—and investigate their evolution with redshift.

The tidal interactions inherent in galaxy mergers produce concentrations of gas in the remnant centers. For major mergers ($m/M \gtrsim 0.3$), models predict that this effect results in a significant burst of increased star formation rate (SFR) compared to the central galaxy's past star formation history (SFH; e.g., Mihos & Hernquist 1996; Cox et al. 2008). It is also likely to enable supermassive black hole growth and the fueling of active galactic nucleus (AGN; e.g., Heckman et al. 1986; Springel et al. 2005; Somerville et al. 2008). Cox et al. (2008) used smooth particle hydrodynamical (SPH) simulations to show that the timescale over which merger-induced starbursts are active depends sensitively on the treatment of poorly understood feedback and interstellar matter (ISM) physics; they demonstrate that future observational constraints on this timescale may provide

a means to constrain feedback models (Barton et al. 2007, and references therein). Historically, SPH simulations have treated star-forming gas as isothermal, and this treatment results in starburst timescales in major mergers that are quite short lived, with $t_* \sim 100$ Myr (e.g., Mihos & Hernquist 1996; Cox et al. 2008). Recently, it has become popular in SPH simulations to impose a stiff equation of state for star-forming gas in order to mimic the effects of a multiphase ISM and to suppress star formation and disk fragmentation (Yepes et al. 1997; Springel & Hernquist 2003; Governato et al. 2007). Cox et al. (2008) showed that a stiff equation of state of this kind significantly lengthens the timescale for starburst activity in major mergers to $t_* \sim 500$ Myr. Below we investigate the evolution of merger fractions with 100 Myr and 500 Myr as a first-order means of addressing the differences between merger-induced starburst fractions in different feedback schemes.

A second observationally relevant consequence of mergers is morphological disturbance. Very large mergers, especially those with moderately low gas fractions, likely play a role in transforming late-type disk galaxies into ellipticals (e.g., Toomre & Toomre 1972; Barnes & Hernquist 1996; Robertson et al. 2006a, 2006b; Burkert et al. 2008). If gas fractions are high in major mergers (as expected at high redshift) then they may play a role in building early disks (Robertson et al. 2006a; Hopkins et al. 2009, 2008; Robertson & Bullock 2008). More common are moderate-size ($m/M > 0.1$) DM halo mergers (Stewart et al. 2008), which can produce morphological signatures such as disk flaring, disk thickening, and ring and bar-like structures in disk galaxies (Barnes & Hernquist 1996; Kazantzidis et al. 2008; Younger et al. 2007; Villalobos & Helmi 2008; Purcell et al. 2009) as well as tidal features seen in massive elliptical galaxies (Feldmann et al. 2008).

Below we explore two possibilities for the evolution of the morphological relaxation time with redshift. First, we explore a case where the remnant relaxation time scales with redshift, approximated by the DM halo dynamical time ($\tau \propto (1+z)^{-\alpha}$, $\alpha \simeq 1.1$–1.5; see below), and second we investigate the possibility that relaxation times remain constant with redshift at $\tau \simeq 500$ Myr. The latter timescale is motivated by the results of Lotz et al. (2008a) who studied outputs from SPH merger simulations of $z = 0$ galaxies in great detail (see Cox et al. 2006, 2008; Jonsson et al. 2006; Rocha et al. 2008, for additional descriptions of these simulations and their analysis). These choices bracket reasonable expectations and allow us to provide first-order estimates for the evolution in the morphologically disturbed fraction with redshift. More simulation work is needed to determine how the relaxation times of galaxy mergers should evolve with redshift, including an allowance for the evolution in approach speeds, galaxy densities, and orbital parameters (if any).

Though not discussed in detail here, a third consequence of mergers is the direct, cumulative deposition of cold baryons (gas and stars) into galaxies. For this question, one is interested in the full merger history of individual objects, rather than the instantaneous merger rate or recent merger fraction. Specifically, one may ask about the total mass that has been deposited by major mergers over a galaxy's history. We focus on this issue in Stewart et al. (2009).

In what follows we use a high-resolution dissipationless cosmological ΛCDM N-body simulation to investigate the merger rates and integrated merger fractions of galaxy DM halos of mass $M = 10^{11}$–$10^{13}\,h^{-1}\,M_\odot$ from redshift $z = 0$ to 4. We adopt the simple technique of monotonic abundance matching in order to associate DM halos with galaxies of a given luminosity or stellar mass (e.g., Kravtsov et al. 2004; Conroy et al. 2006; Berrier et al. 2006; Conroy & Wechsler 2009), and make predictions for the evolution of the galaxy merger rate with redshift.

The outline of this paper is as follows. In Section 2, we discuss the numerical simulation used and the method of merger tree construction, while we present merger statistics for DM halos in Section 3. In Section 4, we discuss the method of assigning galaxies to DM halos both as a function of stellar mass, and alternatively as a function of galaxy luminosity (compared to $L_*(z)$). In Section 5, we present our principle results, which characterize the merger rate of galaxies as a function of redshift, with comparison to observed properties of bright galaxies. We summarize our main conclusions in Section 6.

2. SIMULATION

We use a simulation containing 512^3 particles, each with mass $m_p = 3.16 \times 10^8\,h^{-1}\,M_\odot$, evolved within a comoving cubic volume of $80\,h^{-1}$ Mpc on a side using the Adaptive Refinement Tree (ART) N-body code (Kravtsov et al. 1997, 2004). The simulation uses a flat, ΛCDM cosmology with parameters $\Omega_M = 1 - \Omega_\Lambda = 0.3$, $h = 0.7$, and $\sigma_8 = 0.9$. The simulation root computational grid consists of 512^3 cells, which are adaptively refined to a maximum of eight levels, resulting in a peak spatial resolution of $1.2\,h^{-1}$ kpc (comoving). Here, we give a brief overview of the simulation and methods used to construct the merger trees. They have been discussed elsewhere in greater detail (Allgood et al. 2006; Wechsler et al. 2006; Stewart et al. 2008) and we refer the reader to those papers for a more complete discussion.

Field DM halos and subhalos are identified using a variant of the bound density maxima algorithm (Klypin et al. 1999). A *subhalo* is defined as a DM halo whose center is positioned within the virial radius of a more massive halo. Conversely, a *field halo* is a DM halo that does not lie within the virial radius of a larger halo. The virial radius R and mass M are defined such that the average mass density within R is equal to $\Delta_{\rm vir}$ ($\simeq$337 at $z = 0$) times the mean density of the universe at that redshift. Our halo catalogs are complete to a minimum halo mass of $M = 10^{10}\,h^{-1}\,M_\odot$, and our halo sample includes, for example, ∼15,000(10,000) and 2000(500) field halos at $z = 0(3)$ in the mass bins 10^{11-12} and $10^{12-13}\,h^{-1}\,M_\odot$, respectively.

We use the same merger trees described in Stewart et al. (2008), constructed using the techniques described in Wechsler et al. (2002) and Wechsler et al. (2006). Our algorithm uses 48 stored time steps that are approximately equally spaced in expansion factor between $a = (1+z)^{-1} = 1.0$ and $a = 0.0443$. We use standard terminologies for progenitor and descendant. Any halo at any time step may have any number of progenitors, but a halo may have a single descendant—defined to be the halo in the next time step that contains the majority of this halo's mass. The term *main progenitor* is used to reference the most massive progenitor of a given halo, tracked back in time.

Throughout this work, we present results in terms of the *merger ratio* of an infalling object, m/M, where we always define m as the mass of the smaller object just *prior* to the merger and M is the mass *main progenitor* of the larger object at the same epoch. Specifically, M in the ratio does not incorporate the mass m and therefore m/M has a maximum value of 1.0. Except when explicitly stated otherwise, we always use DM halo masses to

Table 1
Merger Rate Fitting Function Parameters for Equations (1)–(3)

Dark matter halos ($M = 10^{11.0-13.5}\,h^{-1}\,M_\odot$)	$A(z, M)$[a]	c	d
dN/dt: (INFALL) simple fit	$0.020\,(1+z)^{2.3}\,M_{12}^{0.15}$	0.50	1.30
dN/dt: (INFALL) complex fit	$0.020\,(1+z)^{2.3}\,M_{12}^{0.15}$	$0.4 + .05z$	1.30
dN/dz: (INFALL)	$0.27\,(d\delta_c/dz)^2\,M_{12}^{0.15}$	0.50	1.30
dN/dt: (DESTROYED)	$0.022\,(1+z)^{2.2}\,M_{12}^{0.2}$	0.54	0.72
dN/dz: (DESTROYED)	$0.32\,(d\delta_c/dz)\,M_{12}^{0.2}$	0.54	0.72
Galaxy luminosity cuts ($L > f\,L_*, 0.1 < f < 1.0$)	$A(z, f)$[a]	c	d
dN/dt	$0.02\,(1+f)\,(1+z)^{2.1}$	0.54	0.72
Merger fraction in past T (Gyr) (Frac < 0.6, $T < 4$)	$0.02\,T\,(1+f)\,(1+z)^{2.0}$	0.54	0.72
Galaxy stellar mass ranges ($F(x) = F(m_*/M_*)$)	$A(z)$[a]	c_*[b]	d_*[b]
dN/dt ($10^{10.0}\,M_\odot < M_* < 10^{10.5}\,M_\odot$)	$0.015\,e^{1.0z}$	0.30	$1.1 - 0.2z$
dN/dt ($10^{10.5}\,M_\odot < M_* < 10^{11.0}\,M_\odot$)	$0.035\,e^{0.7z}$	0.25	$1.1 - 0.2z$
dN/dt ($10^{11.0}\,M_\odot < M_*$)	$0.070\,e^{1.0z}$	0.20	$1.0 - 0.3z$

Notes.
[a] When not dimensionless, units are Gyr^{-1}.
[b] Mass-ratio variable for galaxy stellar mass merger rates are identified with a *stellar mass* ratio, $r = m_*/M_*$.

define the merger ratio of any given merger event, and we always define the merger ratio as the mass ratio just before the smaller halo falls into the virial radius of the larger one. Because there is not a simple linear relation between halo mass and galaxy stellar (or baryonic) mass, this is an important distinction. For example, our major mergers, defined by halo mass ratios, may not always correspond to major galaxy mergers as defined by stellar or baryonic mass ratios (see, e.g., Stewart 2009).

In what follows we investigate two types of mergers. The first and most robust of our predicted rates is the *infall rate*: the rate at which infalling halos become subhalos, as they first fall within the virial radius of the main progenitor. These are the results we present in Section 3, which describes our "universal" merger rate function for DM halos. The second rate is aimed more closely at confronting observations and is associated with central mergers between galaxies themselves. Specifically we define the *destruction rate* by counting instances when each infalling subhalo loses 90% of the mass it had prior to entering the virial radius of the larger halo.[3] We are unable to measure central crossings directly because the time resolution in our snapshot outputs (typically $\Delta t \simeq 250$ Myr) is comparable to a galaxy–galaxy crossing time at the centers of halos, however, for mergers with mass ratios $>1/3(1/10)$, subhalo destruction typically takes place $\sim$2(3) Gyr after infall to the virial radius. Based on simulations of galaxy mergers, this definition leads to subhalo "destruction" sometime after its first pericenter (and likely after second pericenter), but probably before final coalescence (Boylan-Kolchin et al. 2008). Note that this second rate (destruction) is more uncertain than the first (infall) because, in principle, the orbital evolution of infalling galaxies will depend upon the baryonic composition of both the primary and secondary objects. Fortunately, as presented in detail below (see Table 1) for the relatively high-mass-ratio merger events we consider, the merger rates (and their evolution with redshift) do not depend strongly on whether we define a merger to occur at halo infall or at this central mass-loss epoch.

[3] Subhalo masses are defined to be the mass within a truncation radius R_t, which is set to be the minimum of the virial radius and the radius where the subhalo density profile begins to encounter the background halo density.

3. DARK MATTER HALO MERGER RATES

We begin by investigating infall and destruction merger rates as a function of mass, merger ratio, and redshift. Merger rates are shown for several of these choices in the four panels of Figure 1. The upper panels show merger rates per unit time for $>m/M$ mass-ratio objects falling into host halos of mass 10^{12} (black lines and crosses) and $10^{13}\,h^{-1}\,M_\odot$ (red lines and squares) at three different redshifts: $z = 0$ (solid), $z = 2$ (dashed), and $z = 3$ (dot dashed). Host halo mass bins span $\Delta \log_{10} M = 0.5$, centered on the mass value listed. The upper-left panel presents rates measured at subhalo infall—i.e., the merger rates of distinct halos—and the upper-right panel presents rates of subhalo destruction (when the associated subhalo loses 90% of the mass it had prior to entering the virial radius of the larger halo), which we expect to more closely trace the galaxy merger rates. The lower-left panel presents infall rates, now plotted at a fixed mass ratio ($>m/M = 0.1, ..., 0.7$ from top to bottom) and host mass ($M = 10^{12.5}\,h^{-1}\,M_\odot$, triangles; $M = 10^{11.5}\,h^{-1}\,M_\odot$, squares) as a function of redshift. The same information is presented in the lower-right panel, but now presented as the rate per unit redshift instead of per unit time. We see that merger rates increase with increasing mass and decreasing mass ratio, and that the merger rate per unit time increases with increasing redshift out to $z \sim 4$.

We quantify the measured dependences using simple fitting functions. The merger rate (for both infall and destruction rates) per unit time for objects with mass ratios larger than m/M into halos of mass M at redshift z is fitted using

$$\frac{dN}{dt}(> m/M) = A_t(z, M)\,F(m/M). \quad (1)$$

For the infall rate, we find that the normalization evolves with halo mass and redshift as $A_t(z, M) = 0.02\ \mathrm{Gyr}^{-1}\,(1+z)^{2.2}\,M_{12}^{b}$

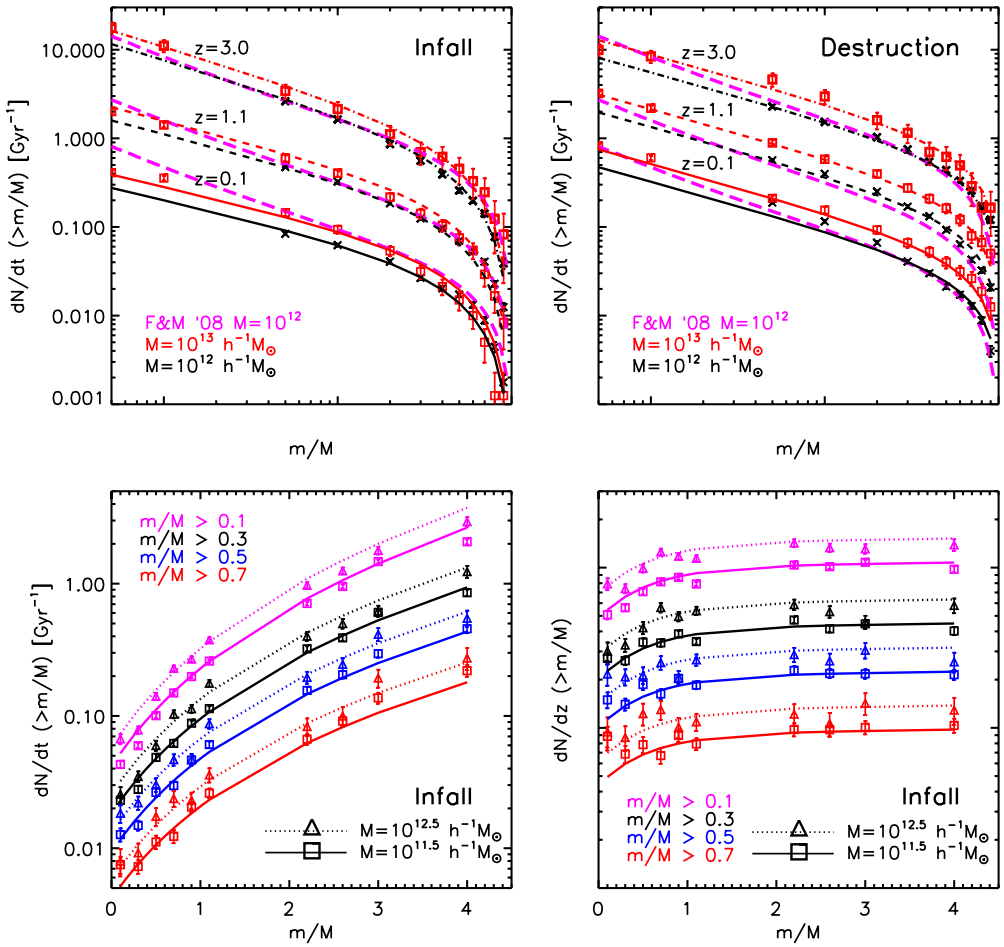

Figure 1. Dark matter halo infall and destruction rates (see Section 2) as a function of mass, merger mass ratio, and redshift. Host halo mass bins span $\Delta \log_{10} M = 0.5$. Top left: infall rate per Gyr as a function of merger mass ratio. The dashed (pink) lines are a comparison to the results of Fakhouri & Ma (2008) for $M = 10^{12}\,h^{-1}\,M_\odot$ (lower) and $M = 10^{13}\,h^{-1}\,M_\odot$ (upper) halos. Top right: identical to top left, but for the destruction rate of halos instead of the infall rate. Bottom left: infall rate per Gyr as a function of redshift. Bottom right: infall rate per unit redshift, as a function of redshift. In the top panels, black and red lines correspond to different host halo masses (10^{12} and $10^{13}\,h^{-1}\,M_\odot$), while in the bottom panels, magenta, black, blue, and red lines correspond to different merger ratios ($m/M > 0.1, 0.3, 0.5, 0.7$). In all panels, the mass ratio, m/M is defined prior to the infall of the smaller system. Error bars are Poissonian based on the number of host halos and the number of mergers. Horizontal error bars on the bottom figures have been omitted for clarity, but are identical to those in Figure 2.

(A color version of this figure is available in the online journal.)

with M_{12} the mass in units of $10^{12}\,h^{-1}\,M_\odot$ and $b = 0.15$. The merger-mass-ratio dependence is fitted by

$$F(m/M) \equiv \left(\frac{M}{m}\right)^c \left(1 - \frac{m}{M}\right)^d, \qquad (2)$$

with $c = 0.5$, and $d = 1.3$. A similar fit describes the destroyed rate, as summarized in Table 1. The fits are illustrated by solid lines that track the simulation points in each of the dN/dt panels in Figure 1.

The solid and dotted lines in the lower-right panel of Figure 1 show that the infall rate per unit redshift, dN/dz, is well described by the same mass-dependent function, but with a normalization that is only weakly dependent on redshift:

$$\frac{dN}{dz}(> m/M) = A_z(z, M)\,F(m/M), \qquad (3)$$

where $A_z(z, M) = 0.27\,(d\delta_c/dz)^2\,M_{12}^{0.15}$ (for infall rate; see Table 1 for destruction rate). As discussed by Fakhouri & Ma (2008, hereafter FM08), a redshift evolution of this form is motivated by the expectations of Extended Press–Schechter theory. Note that since $d\delta_c/dz$ asymptotes to a constant $\sim$1.3 for $z \gtrsim 1$ and evolves only mildly to $\sim$0.9 at $z \simeq 0$, the overall redshift dependence is weak.

To a large extent, our results confirm and agree with those of FM08, who studied merger rates for halos in the Millennium simulation (Springel et al. 2005) and presented a fitting function for the merger rate per unit redshift per unit mass ratio for halos as a function of mass and redshift (the differential of our rate, dN/dz, with respect to the merger rate m/M), and concluded that it was nearly universal in form. For comparison, the pink dashed lines in the top left panel of Figure 1 show the implied expectations based on the FM08 fit for $M = 10^{12}\,h^{-1}\,M_\odot$ (lower lines for each pair) $M = 10^{12}\,h^{-1}\,M_\odot$ (upper lines) halos.[4] The agreement is quite remarkable, especially in light of the fact that the simulation, merger tree algorithm, and halo finder all differed substantially from our own. Note that the agreement is particularly good over the mass ratios $m/M \simeq 0.05$–0.5 that are likely the most important for galaxy formation (in terms of their potential for morphological transformation and overall mass deposition, see Stewart et al. 2008). We note, however, that our infall rate data are smaller than FM08 by a factor of

[4] We use their fit for the "stitching" merger rate, which corresponds most closely to our own definition for halo mergers.

$\sim$1.5 for very large mass-ratio mergers $m/M \gtrsim 0.7$ and by a factor of $\sim$2 for very small mass-ratio mergers $m/M \lesssim 0.01$ (this discrepancy for small mergers is slightly worse at low redshift, $z \lesssim 0.3$). In addition, we find a slightly stronger mass dependence, $dN/dt \propto M^{0.15}$ as opposed to $dN/dt \propto M^{0.1}$ as found by FM08.

It is interesting to note that in an independent analysis of the Millennium simulation, Genel et al. (2008) studied the (infall) merger rates of halos by defining halo masses and mergers in slightly different ways from FM08, in an effort to further remove artifacts of the halo-finding algorithm of the simulation. Among other results, their findings suggested that the merger rates from FM08 are slightly too high (by $\lesssim$50%) for low redshift and for minor ($<1/10$) mergers. This is qualitatively similar to the differences between FM08 and our own results, motivating the need for future study regarding the sensitivity of merger statistics from DM simulation on halo-finding algorithms, as well as halo mass and merger definitions.

Our results also largely agree with an investigation of the major merger rate ($>1/3$ mergers) of halos and subhalos by Wetzel et al. (2009). They found that the infall rate for halos ($M = 10^{11}$–$10^{13}\,h^{-1}\,M_\odot$) evolves with redshift as $dN/dt = A(1+z)^\alpha$ (with $A \sim 0.03$ and $\alpha = 2.0$–2.3) from $z = 0.6$ to 5, in good agreement with our infall rates both in slope and in normalization (see Table 1). Wetzel et al. (2009) also reported on the subhalo merger rate in their simulations (the rate at which satellite subhalos finally merge with the central subhalo) and found similar behavior as field halos for low redshift ($A \sim .02$ and $\alpha \sim 2.3$ for $z = 0.6$–1.6, in good agreement with our destruction rates) but with a significantly flatter slope for high redshift ($A \sim 0.08$ and $\alpha = 1.1$ for $z = 2.5$–5, a factor of 2–3 lower than our results, with a significantly flatter slope). Even though our destruction rate attempts to track a similar physical phenomenon as their subhalo merger rate—the rate of impact of satellite galaxies onto central galaxies—we find destruction rates to show qualitatively similar behavior to infall rates at *all* redshifts.

We speculate that the discrepancy between their results and ours may be due primarily to differences in definition. For example, we define an infalling halo to be "destroyed" once it loses 90% of its infall mass (see Section 2). Wetzel et al. (2009) define subhalo mergers by tracking the evolution of the subhalo's 20 most-bound particles, resulting in a much more stringent definition of a merger, and increasing the time delay between infall to the virial radius ($t_{\rm inf}$) and the time at which the satellite is destroyed ($t_{\rm merge}$). More importantly, we define the merger mass ratio by the halo masses when the satellite halo first falls into the virial radius of the host, $m_{\rm inf}/M_{\rm inf}$. Although we track the subhalo until it has lost 90% of its mass in order to assign a proper *time* that the merger takes place, we do not redefine this merger ratio based on any subsequent growth or decay of either halo. Although Wetzel et al. (2009) define the satellite halo's mass in an identical fashion, they allow for the growth of the central halo during the decay time of the subhalo. Once the subhalo is destroyed, they use the host halo mass at *this* time (minus the mass of the subhalo, so that $m/M < 1$) and thus define the merger ratio as $m_{\rm inf}/M_{\rm merge}$. As a consequence, the host halo has a significant time period ($t_{\rm merge} - t_{\rm inf}$) to grow in mass, leading to smaller mass ratio definitions for identical merger events, as compared to our definition. This effect is likely negligible at late times, when halos do not grow significantly over the $\sim$2 Gyr decay timescales typical for major mergers. This may be why the two studies agree rather well for $z < 1.6$. However, the central halo's mass growth on these timescales becomes increasingly important at high redshift, possibly explaining the flattening of α reported by Wetzel et al. (2009), as compared to our own results.

O. Fakhouri & C. P. Ma (2009, in preparation) investigate this issue to some degree by studying the subhalo merger rate in the Millennium simulation using differing mass-ratio definitions. Whether they implement a merger ratio definition similar to our destruction rate, or one more similar to that of Wetzel et al. (2009), their merger rates remain well fitted to a power law in $(1+z)$, in line with our results. In this case, the underlying cause of the discrepancy between our merger rates (and those of O. Fakhouri & C. P. Ma (2009, in preparation) and the subhalo merger rates reported by Wetzel et al. (2009) remains uncertain. Such comparisons between our respective results highlight the differences that are manifest in defining mergers. When including baryons, properly defining mergers and merger mass ratios becomes even more complicated (see, e.g., Stewart 2009), but even between DM structures, differences such as those found between our work, Wetzel et al. (2009) and O. Fakhouri & C. P. Ma (2009, in preparation) further motivate the need for focused simulations in order to determine the timescales and observational consequences associated with the much more cleanly defined rate with which DM subhalos first fall within the virial radii of their hosts.

4. ASSOCIATING HALOS WITH GALAXIES

While DM halo merger rates at a given mass are theoretically robust quantities to compute in our simulation, they are difficult to compare directly with observations. One particularly simple, yet surprisingly successful approach is to assume a monotonic mapping between DM halo mass M (or similarly the halo maximum circular velocity) and galaxy luminosity L (Kravtsov et al. 2004; Tasitsiomi et al. 2004; Vale & Ostriker 2004; Conroy et al. 2006; Berrier et al. 2006; Purcell et al. 2007; Marín et al. 2008; Conroy & Wechsler 2009). With this assumption, provided that we know the cumulative number density of galaxies brighter than a given luminosity, $n_g(>L)$, we may determine the associated halo population by finding the mass $M(L)$ above which the number density of halos (including subhalos) matches that of the galaxy population $n_h(>M_{\rm DM}) = n_g(>L)$. Table 2 shows the number densities of various galaxy populations from redshifts $z = 0.1$–4 obtained using a variety of surveys for galaxies brighter than $L = f\,L_*$, where $f = 0.1, 0.4$, and 1.0. We list the associated number-density-matched minimum DM halo mass in each case, $M_{\rm DM}$, and we use this association to identify halos with galaxies below. For example, from the top left entry of this table, we see that $n_h(>10^{11.2}\,h^{-1}\,M_\odot) = n_g(>0.1\,L_*)$ at $z = 0.1$.

One important point of caution is that the luminosity functions used to make these assignments at different redshifts vary in rest-frame band, as indicated in Column 2. Specifically, one concern might be that UV luminosity at low redshift is not strongly correlated with DM halo mass, so assuming such a correlation for high-redshift galaxies is not valid. Unlike their low-redshift counterparts, however, there is a strong correlation in high-redshift ($z > 2$) galaxies between star formation and total baryonic mass, as well as a trend for more UV luminous galaxies to be more strongly clustered, suggesting that connecting UV luminosity to halo mass at these redshifts is a valid technique (see discussion in Conroy et al. 2008, and references therein). Encouragingly, as shown in the two $z = 3$ rows, the number

Table 2
Dark Matter Halo Mass–Luminosity Relationship by Number Density Matching

z	Source and Rest-Frame Band	$>0.1\ L_*$		$>0.4\ L_*$		$>L_*$		$\tau(z)$
		n_g[a]	$M_{\rm DM}$[b]	n_g[a]	$M_{\rm DM}$[b]	n_g[a]	$M_{\rm DM}$[b]	(Gyr)
0.1	SDSS ($r^{0.1}$ band)[c]	29	$10^{11.2}$	10	$10^{11.7}$	3.2	$10^{12.3}$	1.79
0.3	COMBO-17/DEEP2 (B band)[d]	20	$10^{11.4}$	5.8	$10^{12.0}$	1.5	$10^{12.6}$	1.50
0.5	COMBO-17/DEEP2 (B band)[d]	24	$10^{11.3}$	7.0	$10^{11.9}$	1.8	$10^{12.5}$	1.28
0.7	COMBO-17/DEEP2 (B band)[d]	20	$10^{11.4}$	5.8	$10^{12.0}$	1.5	$10^{12.6}$	1.09
0.9	COMBO-17/DEEP2 (B band)[d]	25	$10^{11.3}$	7.3	$10^{11.9}$	1.9	$10^{12.5}$	0.95
1.1	COMBO-17/DEEP2 (B band)[d]	19	$10^{11.4}$	5.5	$10^{12.0}$	1.4	$10^{12.5}$	0.81
2.2	Keck Deep Fields (UV)[e]	20	$10^{11.3}$	6.4	$10^{11.7}$	1.8	$10^{12.2}$	0.49
$\sim$2.6	Extrapolation (UV)	$\sim$18	$10^{11.3}$	$\sim$5.2	$10^{11.8}$	$\sim$1.2	$10^{12.3}$	0.40
3	Keck Deep Fields (UV)[e]	15	$10^{11.2}$	3.8	$10^{11.7}$	0.90	$10^{12.2}$	0.32
3	Lyman break galaxies (V band)[f]	NA	NA	5.0	$10^{11.7}$	0.82	$10^{12.2}$	0.32
4	HUDF + *HST* ACS Fields (UV)[g]	18	$10^{11.0}$	3.2	$10^{11.6}$	0.61	$10^{12.0}$	0.25

Notes.
[a] $10^{-3}\,h^3$ Mpc^{-3}.
[b] $h^{-1}\,M_\odot$.
[c] Blanton et al. (2003).
[d] Faber et al. (2007) with DEEP2 optimal weights.
[e] Sawicki & Thompson (2006).
[f] Shapley et al. (2001)—note that rest-frame V number densities match well with $> 0.4\ L_*$ and $> L_*$ values in rest UV at $z = 3$.
[g] Bouwens et al. (2007).

densities of $f\ L_*$ galaxies from Sawicki & Thompson (2006; rest-frame UV) and Shapley et al. (2001; rest-frame V) are quite similar.

We also note that the data from these various sources will contain uncertainties in the number counts of galaxies from, e.g., cosmic variance. For example, the COMBO17/DEEP2 data fluctuate about a nearly constant value ($\sim$0.02–0.03 h^3 Mpc^{-3}) from $z = 0.3$ to 1.1, suggesting a $\sim$30% uncertainty in these values. We find that a 30% error in the observed number density typically translates into a similar 30% error in the assigned minimum halo mass in our simulation. Since DM halo merger rates are only weakly dependent on halo mass ($\propto M_{\rm DM}^{0.2}$), this should result in only a $\sim$10% uncertainty in our merger rates. Thus, the merger rates we present here should be relatively robust to small errors in observational uncertainties. For example, if we adopt minimum halo masses (regardless of redshift) of $M_{\rm DM} = 10^{11.2}$, $10^{11.7}$, and $10^{12.3}\,h^{-1}\,M_\odot$ as corresponding to $>$0.1, 0.4, and 1.0 L_* galaxies, respectively, our resulting merger rates change by $<$25% (typically 5%–15%).

A related approach is to use observationally derived stellar mass functions and to assume a monotonic relationship between halo mass and stellar mass M_*. Though a monotonic relationship between total stellar mass and DM mass avoids the issue of color band that arises in luminosity mapping, we cannot use it explore merger rates as a function of stellar mass above $z \sim 2$ because the stellar mass function is poorly constrained beyond moderate redshifts. For our analysis, we will adopt the relation advocated by Conroy & Wechsler (2009, hereafter CW09; interpolated from the data shown in their Figure 2). For example, CW09 find that the halo mass M associated with stellar masses of $M_* = (1, 3, 10) \times 10^{10}\ M_\odot$ at $z = 0, 1, 2$ are $M(z = 0) \simeq (2.5, 7.0, 47) \times 10^{11}\,h^{-1}\,M_\odot$; $M(z = 1) = (4.0, 9.6, 41) \times 10^{11}$; and $M(z = 2) = (2.1, 3.9, 10) \times 10^{12}\,h^{-1}\,M_\odot$. We note that because this mapping between stellar mass and halo mass is not well fitted by a constant ratio, $M_* = f\,M_{\rm DM}$, merger rates in terms of *stellar* mass ratios show qualitatively different evolution with redshift (see Section 5.1). This is primarily because mergers of a fixed DM mass ratio do *not* typically correspond to the same stellar mass ratio (see Stewart 2009).

Note that while the DM halo merger rates presented in Section 3 give robust theoretical predictions, the merger rates we will present in terms of luminosity (or stellar mass) are sensitive to these mappings between halo mass and L (or M_*). In addition, it is difficult to perform a detailed investigation into the errors associated with these mappings, as there are inherent uncertainties in the luminosity and stellar mass functions, especially at $z > 1$. It is also possible that the monotonic mapping between halo mass and L (or M_*) may break down at $z > 1$ (see discussion in CW09). These uncertainties must be kept in mind when comparing our predicted merger rates (in terms of L or M_*) to observations, especially at high redshift. Nevertheless, the halo masses we have associated with a given relative brightness should be indicative.

5. GALAXY MERGER PREDICTIONS

5.1. Merger Rates

Our predicted merger rates (per galaxy, per Gyr) and their evolution with redshift, averaged over $L > L_*$ and $L > 0.1\ L_*$ galaxy populations, are illustrated in the left and middle panels of Figure 2. Rates are presented for a few selected *DM halo* mass-ratio cuts $m/M > 0.1$, 0.3, 0.5, and 0.7. Here, galaxy merger rates are defined using the *destruction rate*, when the infalling subhalo is identified as destroyed in the simulation (see Section 2). The solid lines correspond to a fit in the form of Equation (1), with the normalization evolving as $A_t(z, f) \propto (1 + f)(1 + z)^{2.1}$ for $L > f\ L_*$ galaxies. The explicit best-fit parameters for the merger rate as a function of luminosity cut are given in Table 1.

For comparison, the right panel in Figure 2 shows the predicted evolution in the merger rates per galaxy for two bins of stellar mass, according to the CW09 mapping described above: $10^{10.0}\,M_\odot < M_* < 10^{10.5}\,M_\odot$ (lower, blue) and $M_* > 10^{11}\,M_\odot$ (upper, red). Shown are merger rates for two choices of *stellar mass* ratio mergers, $(m_*/M_*) > 0.3$, 0.6 (solid and dashed lines, respectively). The solid and dashed lines correspond to fits to our simulation results in the form of Equation (1), with $A_t(z) \propto e^{1.2z}$. The explicit best-fit parameters for these two

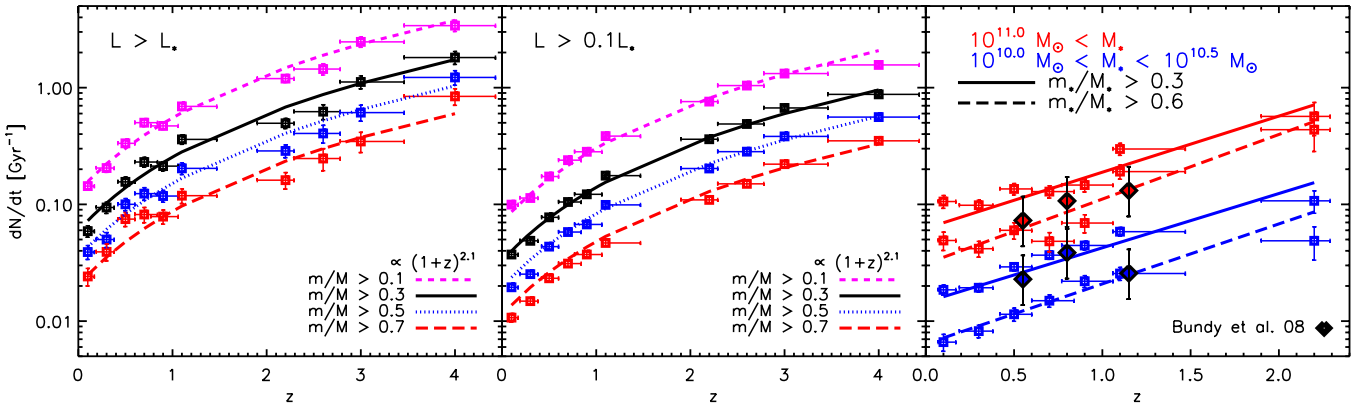

Figure 2. Expected merger rates per Gyr for galaxies of an indicated type as a function of redshift. The vertical error bars show Poisson errors on both the number of main halos and the total number of mergers averaged over per redshift bin while the horizontal error bars show the redshift bins used to compute the merger rate at each redshift. The error bars do not include uncertainties in the mapping of mass to luminosity or stellar mass. Left: merger rate into galaxies with $L > L_*$ involving objects with *total* mass ratios $m/M > 0.1, ..., 0.7$ as indicated. Middle: merger rate into galaxies with $L > 0.1\ L_*$. Right: merger rates for galaxies of a given *stellar* mass involving objects with *stellar mass ratios* $m_*/M_* > 0.3$ and 0.6 as a function of redshift. (Note that the redshift range in this panel only goes to $z = 2$.) We include two different stellar mass cuts in this panel, represented by the red and blue lines. The dotted lines in this panel show an extrapolation out to $z \sim 4$, based on our fit to the $z < 2$ simulation data. The filled diamonds show observational results for the same stellar mass cuts from Bundy et al. (2009).

(A color version of this figure is available in the online journal.)

stellar mass bins (as well as an intermediate bin, $10^{10.5}\ M_\odot < M_* < 10^{11.0}\ M_\odot$) can be found in Table 1. Table 1 also provides best-fit parameters for the function $F(r)$ (Equation 2) where now we associate the ratio r with the stellar mass ratio $r = m_*/M_*$. Note that we only show our simulation points for $z \lesssim 2$ in this panel, due to uncertainties in the stellar mass function at high redshift.

While the galaxy merger rate cannot be observed directly, it can be inferred using a number of different techniques. Mergers that are about to occur may be forecast by counting galaxy close pairs, and close pair fractions are often used as a proxy for the merger rate. The filled diamonds in the right panel of Figure 2 are recent merger-rate estimates from the pair count study of Bundy et al. (2009), for the same two stellar mass bins shown in the simulations (blue for the lower mass bin, red for the upper mass bin). Bundy et al. (2009) have used the simulation results of Kitzbichler & White (2008) to derive merger rates from the observed pair fraction. Overall, the trends with mass and redshift are quite similar and this is encouraging. However, the Bundy et al. (2009) results correspond to mergers with stellar mass ratios larger than $m_*/M_* \gtrsim 0.25$. Our normalization is a factor of ∼2 too high compared to this, and only matches if we use larger merger ratios $m_*/M_* \gtrsim 0.5$. It is possible that this mismatch is associated with the difficulty in assigning merger timescales to projected pairs (see, e.g., Berrier et al. 2006). It may also be traced back to uncertainties in assigning stellar masses to DM halo masses, however, since merger rates have relatively weak dependence on halo mass, it would require increasing our assigned stellar masses by a factor of ∼3 in order to account for this discrepancy solely by errors in assigning stellar mass (such an increase in stellar mass would result in unphysical baryonic content for DM halos: e.g., $10^{12}\ h^{-1}\ M_\odot$ halo containing $M_* > 10^{11}\ h^{-1}\ M_\odot$).

There are a number of other observational estimates of the merger rate based on pair counts of galaxies (e.g., Patton et al. 2002; Lin et al. 2004; Bell et al. 2006; Kartaltepe et al. 2007; Kampczyk et al. 2007; de Ravel et al. 2009; Lin et al. 2008; McIntosh et al. 2008; Patton & Atfield 2008; Ryan et al. 2008). We choose to compare our results to Bundy et al. (2009) as a recent representative of such work, primarily because it is more straightforward for us to compare to samples that are defined at a fixed stellar mass and stellar mass ratio. It is also difficult to compare to many different observational results on the same figure self-consistently, because different groups adopt slightly different cuts on stellar mass (or luminosity) and on mass ratios for pairs. We note that if we were to extrapolate our best-fit curves to higher redshift than our data ($z \sim 4$), we find good agreement between our simulation data and the merger rate estimates using CAS (concentration, asymmetry, clumpiness) morphological classifications from Conselice et al. (2003) for galaxies with $M_* > 10^{10}\ h^{-1}\ M_\odot$. However, the mapping between stellar mass and halo mass adopted from CW09 is only valid to $z = 2$ (and most robust for $z < 1$), so extrapolating these fits to $z \sim 4$ is only a first-order check, and should not be considered a reliable prediction.

5.2. Merger Fractions

Another approach in measuring galaxy merger rates is to count galaxies that show observational signatures of past merging events such as enhanced star formation, AGN activity, and morphological disturbances. Unfortunately, the timescale over which any individual signature will be observable is often extremely uncertain, and will depend on the total mass and baryonic makeup of the galaxies involved as well as many uncertain aspects of the physics of galaxy formation (e.g., Berrier et al. 2006; Cox et al. 2008; Lotz et al. 2008a; Kitzbichler & White 2008). In order to avoid these uncertainties, we present results for merger fractions using several choices for look-back timescale here.

The three panels of Figure 3 show the predicted evolution of the merger fraction in galaxies brighter than 0.4 L_* for three different choices of merger look-back time and for various choices for the total mass merger fraction $m/M > 0.1, ..., 0.7$. The horizontal error bars on this figure show the *actual* redshift bins used to compute the merger fractions. The left and right panels show the merger fraction within 100 Myr and 500 Myr, respectively,[5] and the middle panel shows the fraction of

[5] In most cases, the available time steps ($\Delta t \simeq 250$ Myr) are too widely spaced to directly measure fractions within 100 Myr. For this reason, the left panel is actually the merger fraction within the last Δt time step, scaled down by a factor of $(\Delta t/100\,\mathrm{Myr}) \simeq 2.5$.

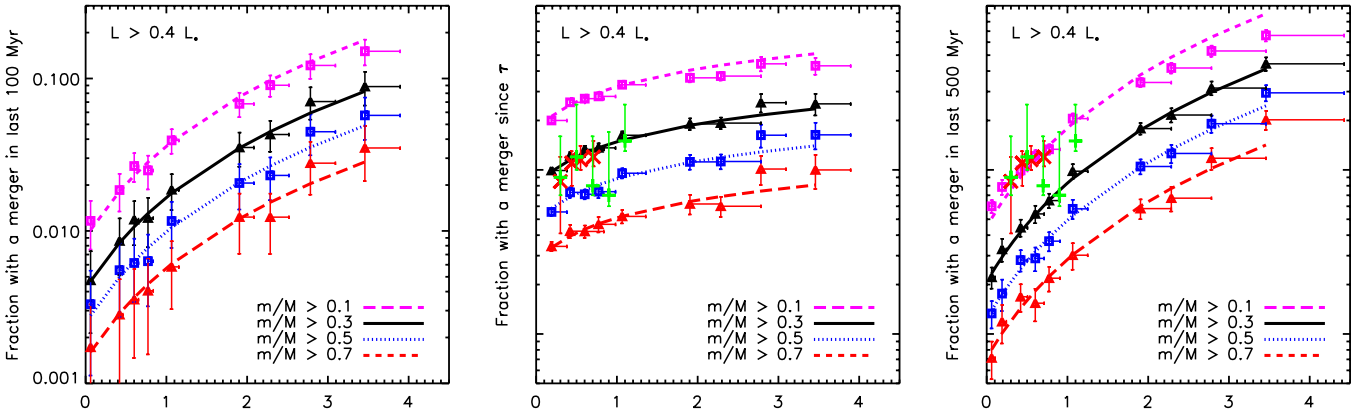

Figure 3. Fraction of halos that experience at least one merger larger than m/M in the past 100 Myr (left), halo dynamical time τ (middle), or 500 Myr (right), as a function of z. Error bars show the Poisson $\sqrt{N}$ error based on the both the number of main halos and the total number of mergers averaged over, while the horizontal error bars show the redshift bins used to compute the merger rate at each redshift. The error bars do not include uncertainties in the mapping of mass to luminosity. The symbols represent estimates of the observed merger fraction at various redshifts, based on Jogee et al. (2008, red crosses) and Lotz et al. (2008b, green plus signs), respectively.

(A color version of this figure is available in the online journal.)

galaxies that have had a merger within the past halo dynamical time[6] $\tau(z)$, where $\tau(z) \simeq 2.0$ Gyr $(1+z)^{-1.15}$ for $z \leqslant 1$ and $\tau(z) \simeq 2.6$ Gyr $(1+z)^{-1.5}$ for $z > 1$.

5.2.1. Merger-driven Starbursts

Several recent studies of SFRs in galaxies at $z = 0$–1 suggest that the cosmic SFR density is not dominated by strongly disturbed systems with brief periods of intense star formation, as might be expected if merger-driven starbursts are common. Instead, the SFR density appears to be dominated by normal, non-merging galaxies (Wolf et al. 2005; Bell et al. 2005; Jogee et al. 2008; Noeske et al. 2007). That is, $< 30\%$ of the instantaneous SFR density at a given redshift (from $z = 0$ to 1) is derived from morphologically disturbed galaxies, which may be currently undergoing a merger-induced starburst. Even at high redshift ($z \sim 2$), a comparison of the clustering of star-forming galaxies to that of DM halos suggests that these galaxies are consistent with massive galaxies (in massive DM halos) quiescently forming stars, as opposed to less massive galaxies (less massive DM halos) in the midst of merger-induced starbursts (Conroy et al. 2008). However, this conclusion is based on the assumption that UV-bright galaxies at this redshift comprise a representative sample of star-forming galaxies.

As discussed in Section 1, the briefest timescales we expect for merger-triggered starbursts is ∼100 Myr (Mihos & Hernquist 1996; Cox et al. 2008), and for these models we expect the SFR to increase to ∼20 times the isolated value for $m/M \gtrsim 0.3$ events (Cox et al. 2008). (While we adopt these timescales as "typical" of galaxy mergers, it is important to keep in mind that Cox et al. (2008) focus on $z = 0$ galaxies. High-redshift galaxies should typically contain higher gas fractions, which may impact the properties of merger-induced starbursts at these epochs.) As we see from the left panel of Figure 3, the fraction of galaxies that have a merger large enough ($m/M > 0.3$) to trigger such a burst is quite small, $\lesssim$1% for $z \lesssim 1$. It is therefore not surprising that stochastic starbursts of this kind do not dominate the SFR density at moderate to low redshifts. Even at higher redshift ($z = 3$–4), the fraction of galaxies with major mergers on these timescales is less than ∼6% of the total bright galaxy population (consistent with the results presented in Somerville et al. (2008), for their semianalytic model). However, galaxy gas fractions are expected to increase with redshift (Erb et al. 2006), which could presumably result in significant starburst activity from more minor mergers (as well as providing fresh gas accretion in a more cumulative sense, see Stewart et al. 2009). A higher fraction of galaxies have experienced such minor ($>1/10$) mergers on these timescales at $z = 3$–4 (∼15%).

Alternatively, if merger-driven starbursts remain active for ∼500 Myr, as other models suggest, then their enhancements are expected to be less pronounced (with an SFR ∼5 times isolated; Cox et al. 2008). In this case, the right panel of Figure 3 is the relevant prediction, and we see that (at most) ∼3%–9% of bright galaxies could exhibit signs of such elevated SFR activity between $z = 0$ and $z = 1$. It seems that in either case, we would not expect merger-triggered activity to play a major role in driving the integrated SFR at these epochs. Only at the highest redshifts $z \gtrsim 3$ would this seem possible. However, we once again point out that the detailed study of Cox et al. 2008, which we have quoted here, focuses on low-redshift galaxies, with gas fractions <30%. If minor mergers with very high gas fractions (>50%) are capable of triggering starbursts, then over half of all bright galaxies at $z > 2$ (where such high gas fractions are more common) may be in the process of starbursting.

Under the presumption that only major mergers trigger starbursts, we note that our numbers are an upper limit on the fraction of bright galaxies that could be experiencing merger-induced starbursts, because moderately high gas fractions are also necessary. For example, a study of 216 galaxies at $z \sim 2$–3 by Law et al. (2007b) found that galaxy morphology (in rest-frame UV) was not necessarily correlated with SFR, and in a recent examination of two Chandra Deep Field South sources using adaptive optics, Melbourne et al. (2005) found an example of a merger of two evolved stellar populations, in which the major merger signature was not accompanied by a burst of star formation, presumably because both galaxies were gas poor. Lin et al. (2008) find that ∼8% (25%) of mergers at $z \sim 1.1$ (0.1) are gas poor, suggesting that this issue, while less dominant at high redshift, is a significant effect and must be taken into consideration.

[6] We use $\tau = R/V \propto (\Delta_v(z)\,\rho_u(z))^{-1/2}$, such that the halo dynamical time is independent of halo mass.

We note that we have focused on galaxies which are in the *midst* of a merger-induced starburst. The lingering impact these bursts will have on the cumulative SFHs of galaxies in a separate issue entirely. A recent study by Cowie & Barger (2008) traced recent star formation in >2000 galaxies from $z = .05$ to 1.5 and found that roughly a quarter of these galaxies showed color indications (AB3400-AB8140 versus EW in Hβ) indicative of starbursts in the past 0.3–1.0 Gyr. Once again, we find our predictions to be broadly consistent with this result, with ∼20% of bright galaxies (>0.4 L_*) having experienced a major merger in the past Gyr at $z \sim 1$. With this study of individual galaxies' SFHs emphasizing the importance of starbursts, and the previously mentioned studies of the global SFR density emphasizing the importance of star formation in normal, non-merging systems, we find that our predicted merger rates are broadly consistent with both results, suggesting that while starbursts may not be the globally dominant form of star formation in the universe, they still play an important role in the SFHs of galaxies. Detailed progress in understanding the full importance of merger-induced starbursts on the global SFR density of the universe will require a better understanding of the timescales and signatures associated with galaxy mergers and merger-induced starbursts.

5.2.2. Morphological Signatures

Even if the contribution to the overall SFR due to very recent mergers remains low, this does not necessarily imply that there would be a lack of morphological signature. The timescale for morphological relaxation may be significantly longer than starburst activity. Though the precise timescales for relaxation are uncertain, the middle and right panels of Figure 3 explore merger fractions for two reasonable choices: a fixed 500 Myr timescale and a redshift-dependent halo dynamical time τ.

Lotz et al. (2008b) used AEGIS survey data to study the morphological evolution and implied galaxy merger fraction from redshift $z = 0.2$ to 1.2. The merger fraction results for >0.4 L_* galaxies from Lotz et al. (2008b) are shown by the green pluses in the middle and right panels of Figure 3. In a similar investigation, Jogee et al. (2008) study $z = 0.2$–0.8 galaxies using a combination of *Hubble Space Telescope* (*HST*), Advanced Camera for Surveys (ACS), COMBO-17, and *Spitzer* 24 μm data to estimate the fraction of "strongly disturbed" galaxies. Their results[7] are shown by the red crosses in Figure 3, and are in reasonably good agreement with the points from Lotz et al. (2008b). We note that the data from these very recent works seem to be in good agreement with the $m/M > 0.3$ merger fraction if the relaxation time is close to τ. This case in particular has a fairly weak evolution because τ is decreasing with time. Interestingly, however, due to the rather large measurement uncertainties, the data are also in reasonable agreement with the fixed relaxation timescale case of 500 Myr (which has a steeper evolution with z), as long as more minor mergers ($m/M > 0.1$) can trigger the observed activity. The fact that the data match both the predictions in the middle panel and right panel of Figure 3 draws attention to the inherent degeneracies in this comparison. The same merger fractions are obtained with high-mass-ratio merger events and look-back times or with lower mass-ratio mergers with slightly shorter look-back times.

[7] The data from Jogee et al. (2008) correspond to a fixed stellar mass cut at $M_* \sim 2.5 \times 10^{10}\ M_\odot$, but the associated dark matter halo mappings from CW09 are close to those for galaxies with >0.4 L_* (see Table 1 and our discussion in Section 4).

We may also compare our predictions with the results of Melbourne et al. (2008), who imaged 15 $z \sim 0.8$ luminous infrared galaxies (LIRGs) with the Keck Laser Guide Star (LGS) AO facility, and found that 3/15 of the galaxies showed evidence for a *minor* merger, while only 1/15 was consistent with a major merger. These results match our expectations for major ($m/M > 0.3$) and minor ($m/M > 0.1$) merger fractions at $z \sim 0.8$ fairly well, considering the small number statistics. Similarly, Shapiro et al. (2008) study 11 rest-frame UV/optical-selected $z \sim 2$ galaxies with spectroscopic data from SINFONI on the VLT, and estimate that ∼25% of these systems are likely undergoing a major (mass ratio $\leqslant$ 3:1) merger. Again, our expectations as shown in the middle and right panels of Figure 3 are consistent with these numbers.

The above discussion makes it clear that meaningful comparisons between observed morphologically disturbed fractions and predicted merger fractions rely fundamentally on understanding how the mass ratio involved affects the morphological indicator and on the associated relaxation timescales of the associated remnants. In addition, merger rates are expected to depend sensitively on the galaxy luminosity and redshift (see Table 1). Comparisons between observational results and theory therefore require great care, especially as it concerns the evolution of the merger rate. If, for example, higher redshift measurements are biased to contain brighter galaxies than lower redshift measurements, then the redshift evolution will likely be steeper than the underling halo merger rate at fixed mass. Or, if higher redshift measurements are sensitive to only the most massive mergers, while lower redshift measurements detect more subtle effects, then the evolution in the merger rate will be biased accordingly.

5.2.3. High-Redshift Expectations

As seen clearly in Figures 2 and 3, the merger rate per galaxy and the corresponding merger fraction at a fixed time are expected to rise steadily toward high redshift. Even after normalizing by the halo dynamical time, which decreases with redshift, this evolution with redshift persists, as seen in Figure 3 (middle). This point is emphasized in Figure 4, which shows the fraction of $L > 0.4\ L_*$ galaxies that have had a merger larger than $m/M = 0.3$ within the last t Gyr (right) and within the last $t/\tau(z)$ (left). The left-hand panel scales out the evolution in the halo dynamical time. We see that ∼50% of $z = 3$ galaxies are expected to have had a major merger in the last 700 Myr, and that these galaxies are ∼4 times as likely to have had a significant merger in the last dynamical time than bright galaxies at $z = 0$. It would be surprising then if mergers did not play an important role in setting the properties of most $z = 3$ galaxies like Lyman break galaxies (LBGs). These major mergers should (at least) deliver a significant amount of gas to fuel star formation, affect LBG dynamics, and perhaps trigger starburst activity. If LBGs represent a biased sample at $z = 3$ (of unusually bright galaxies, more likely to have recently undergone a merger-induced starburst)[8] then it may be possible that the merger fraction in LBGs is even higher than the global merger fraction for >0.4 L_* galaxies.

At higher redshifts, $z > 3$, we expect major mergers to become increasingly common. The brightest galaxies $L > 0.4\,L_*$ should be undergoing mergers frequently, with an overwhelming majority of $z = 4$ galaxies having experienced some significant merger activity in the last ∼500 Myr.

[8] It is estimated that ∼75% of all bright galaxies at $z \sim 3$ are LBGs (Marchesini et al. 2007; Quadri et al. 2007).

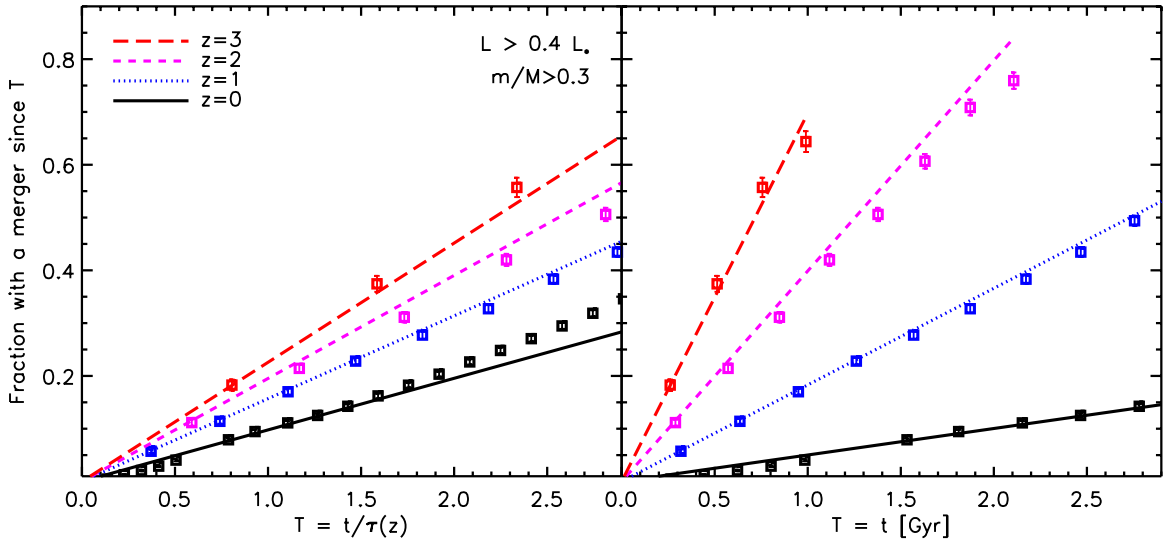

Figure 4. Fraction >0.4 L_* galaxies at $z \sim 0,\ 1,\ 2,$ and 3 (black solid to red dashed lines) that have experienced a major merger ($m/M > 0.3$) over a given time period. Symbols show the simulation data, while the lines are given by the fit in Table 1. Left: merger fraction since t, normalized by the halo dynamical time at each redshift, $\tau(z = 0,\ 1,\ 2,\ 3) \simeq 1.95,\ 0.92,\ 0.49, 0.32$ Gyr. Right: merger fraction in the past t Gyr. Error bars show the Poisson $\sqrt{N}$ error based on the total number of mergers, and are comparable to the symbol sizes. The error bars do not take uncertainties in the mapping of mass to luminosity into account.
(A color version of this figure is available in the online journal.)

6. CONCLUSION

We have used a high-resolution ΛCDM N-body simulation to investigate the instantaneous merger rate of DM halos as a function of redshift (from $z = 0$ to 4), merger mass ratio, and host halo mass from $M = 10^{11}$–$10^{13}\,h^{-1}\,M_\odot$. Merging companions as small as $m = 10^{10}\,h^{-1}\,M_\odot$ were tracked. We use number density matching to associate galaxies with DM halos and present predictions for the merger rate and merger fraction as a function of galaxy luminosity and stellar mass. The principle goal has been to present raw merger statistics that can be compared directly to observations of galaxies to high redshift. Fitting functions that describe our results as a function of luminosity, mass, mass ratio, and redshift are provided in Table 1.

Our main results may be summarized as follows.

1. A simple fitting function describes the accretion rate of small DM halos of mass m into larger DM halos of mass M as a function redshift: $dN/dt = A(z, M)\,F(m/M)$, where typically $A(z, M) \propto (1+z)^{2.2} M^{0.15}$ and $F(m/M) = (M/m)^c(1 - m/M)^d$. Fit parameters for merger rates in terms of dark halo mass, luminosity, or stellar mass are given in Table 1.
2. The merger rate of galaxies of luminosities $L > f\ L_*$ should evolve in a similar manner, with a redshift and luminosity dependence that follows $A(z, f) \propto (1 + f)\ (1 + z)^{2.1}$.
3. Only a small fraction (0.5% at $z = 0$, 10% at $z = 4$) of bright ($> 0.4\ L_*$) galaxies should have experienced a major (> 0.3) merger in their very recent history (100 Myr; Figure 3 left panel). Even if mergers trigger the kind of short-lived, highly efficient star formation bursts that are expected in some models, they cannot contribute significantly to the overall distribution of SFRs at any given epoch.
4. The predicted fraction of galaxies with a merger in the past 500 Myr, or alternatively within a past halo dynamical time, are in reasonable agreement with the fraction of galaxies that show observational signs of morphological disturbance between redshifts $z = 0$ and 2 (Figure 3, middle and left panels). We emphasize, however, that comparisons between theory and observations suffer from significant uncertainties associated with mass-ratio dependences and relaxation timescales.
5. Galaxy merger rates should depend on at least three parameters: mass (or luminosity), merger mass ratio, and redshift (see Table 1). Therefore, any attempt to compare two observational indicators of the merger rate or to relate specific observations to theoretical predictions must take great care in the respective comparisons.
6. Mergers must become increasingly important in shaping galaxy properties at $z > 3$. At $z = 3$, the fraction of galaxies with a merger in the past dynamical time is ∼4 times higher than at $z = 0$. We expect ∼30% (60%) of >0.4 L_* galaxies to have experienced a $m/M > 0.3$ major ($m/M > 0.1$ minor) merger in the past 500 Myr at $z = 3$. Though it is unlikely that short-lived starbursts associated with these mergers drive the increase in the global SFR of galaxies with redshift, the broader implications of these mergers (fresh supply of gas brought in to the central galaxy through accreted satellites, etc.) are undoubtedly linked to star formation and the general growth of galaxies on longer timescales.

The simulation used in this paper was run on the Columbia machine at NASA Ames. We thank Anatoly Klypin for running the simulation and making it available to us. We are also indebted to Brandon Allgood for providing the merger trees. We thank Charlie Conroy for providing us the abundance-matching data from CW09, and Kevin Bundy for providing us with an advance copy of his paper before publication. We thank Jeff Cooke, David Law, Lihwai Lin, Ari Maller, David Patton, Brant Robertson, and Andrew Wetzel for useful discussions. We also thank the anonymous referee, whose insightful comments helped us improve the quality of this paper. J.S.B. and K.R.S. are supported by NSF grant AST 05-07916. K.R.S., J.S.B.,

and E.J.B. received additional support from the Center for Cosmology at the University of California, Irvine. R.H.W. was supported in part by the U.S. Department of Energy under contract number DE-AC02-76SF00515 and by a Terman Fellowship from Stanford University.

REFERENCES

Allgood, B., Flores, R. A., Primack, J. R., Kravtsov, A. V., Wechsler, R. H., Faltenbacher, A., & Bullock, J. S. 2006, MNRAS, 367, 1781
Barnes, J. E., & Hernquist, L. 1996, ApJ, 471, 115
Barton, E. J., Arnold, J. A., Zentner, A. R., Bullock, J. S., & Wechsler, R. H. 2007, ApJ, 671, 1538
Bell, E. F., Phleps, S., Somerville, R. S., Wolf, C., Borch, A., & Meisenheimer, K. 2006, ApJ, 652, 270
Bell, E. F., et al. 2005, ApJ, 625, 23
Berrier, J. C., Bullock, J. S., Barton, E. J., Guenther, H. D., Zentner, A. R., & Wechsler, R. H. 2006, ApJ, 652, 56
Blanton, M. R., et al. 2003, ApJ, 594, 186
Blumenthal, G. R., Faber, S. M., Primack, J. R., & Rees, M. J. 1984, Nature, 311, 517
Bouwens, R. J., Illingworth, G. D., Franx, M., & Ford, H. 2007, ApJ, 670, 928
Boylan-Kolchin, M., Ma, C.-P., & Quataert, E. 2008, MNRAS, 383, 93
Bundy, K., Fukugita, M., Ellis, R. S., Targett, T. A., Belli, S., & Kodama, T. 2009, ApJ, 697, 1369
Burkert, A., Naab, T., Johansson, P. H., & Jesseit, R. 2008, ApJ, 685, 897
Carlberg, et al. 2000, ApJ, 532, L1
Cole, S., Helly, J., Frenk, C. S., & Parkinson, H. 2008, MNRAS, 383, 546
Conroy, C., Shapley, A. E., Tinker, J. L., Santos, M. R., & Lemson, G. 2008, ApJ, 679, 1192
Conroy, C., & Wechsler, R. H. 2009, ApJ, 696, 620
Conroy, C., Wechsler, R. H., & Kravtsov, A. V. 2006, ApJ, 647, 201
Conselice, C. J., Bershady, M. A., Dickinson, M., & Papovich, C. 2003, AJ, 126, 1183
Cowie, L. L., & Barger, A. J. 2008, ApJ, 686, 72
Cox, T. J., Jonsson, P., Primack, J. R., & Somerville, R. S. 2006, MNRAS, 373, 1013
Cox, T. J., Jonsson, P., Somerville, R. S., Primack, J. R., & Dekel, A. 2008, MNRAS, 384, 386
Davis, M., Efstathiou, G., Frenk, C. S., & White, S. D. M. 1985, ApJ, 292, 371
de Ravel, et al. 2009, A&A, 498, 379
Erb, D. K., Steidel, C. C., Shapley, A. E., Pettini, M., Reddy, N. A., & Adelberger, K. L. 2006, ApJ, 646, 107
Faber, S. M., et al. 2007, ApJ, 665, 265
Fakhouri, O., & Ma, C.-P. 2008, MNRAS, 386, 577
Feldmann, R., Mayer, L., & Carollo, C. M. 2008, ApJ, 684, 1062
Förster Schreiber, N. M., et al. 2006, Messenger, 125, 11
Genel, S., Genzel, R., Bouché, N., Naab, T., & Sternberg, A. 2008, arXiv:0812.3154
Genzel, R., et al. 2006, Nature, 442, 786
Gottlöber, S., Klypin, A., & Kravtsov, A. V. 2001, ApJ, 546, 223
Governato, F., Gardner, J. P., Stadel, J., Quinn, T., & Lake, G. 1999, AJ, 117, 1651
Governato, F., Willman, B., Mayer, L., Brooks, A., Stinson, G., Valenzuela, O., Wadsley, J., & Quinn, T. 2007, MNRAS, 374, 1479
Heckman, T. M., Smith, E. P., Baum, S. A., van Breugel, W. J. M., Miley, G. K., Illingworth, G. D., Bothun, G. D., & Balick, B. 1986, ApJ, 311, 526
Hopkins, P. F., Cox, T. J., Younger, J. D., & Hernquist, L. 2009, ApJ, 691, 1168
Hopkins, P. F., Hernquist, L., Cox, T. J., Younger, J. D., & Besla, G. 2008, ApJ, 688, 757
Jogee, S., et al. 2008, in ASP Conf. Ser. 396, Formation and Evolution of Galaxy Disks, ed. J. G. Funes & E. M. Corsini (San Francisco, CA: ASP), 337
Jonsson, P., Cox, T. J., Primack, J. R., & Somerville, R. S. 2006, ApJ, 637, 255
Kampczyk, P., et al. 2007, ApJS, 172, 329
Kartaltepe, J. S., et al. 2007, ApJS, 172, 320
Kazantzidis, S., Bullock, J. S., Zentner, A. R., Kravtsov, A. V., & Moustakas, L. A. 2008, ApJ, 688, 254
Kitzbichler, M. G., & White, S. D. M. 2008, MNRAS, 391, 1489
Klypin, A., Gottlöber, S., Kravtsov, A. V., & Khokhlov, A. M. 1999, ApJ, 516, 530
Kravtsov, A. V., Berlind, A. A., Wechsler, R. H., Klypin, A. A., Gottlöber, S., Allgood, B., & Primack, J. R. 2004, ApJ, 609, 35
Kravtsov, A. V., Klypin, A. A., & Khokhlov, A. M. 1997, ApJS, 111, 73
Kriek, et al. 2008, ApJ, 677, 219
Law, D. R., Steidel, C. C., Erb, D. K., Larkin, J. E., Pettini, M., Shapley, A. E., & Wright, S. A. 2007a, ApJ, 669, 929
Law, D. R., Steidel, C. C., Erb, D. K., Pettini, M., Reddy, N. A., Shapley, A. E., Adelberger, K. L., & Simenc, D. J. 2007b, ApJ, 656, 1
Lin, L., et al. 2004, ApJ, 617, L9
Lin, et al. 2008, in ASP Conf. Ser. 399, Panoramic Views of Galaxy Formation and Evolution, ed. T. Kodama, T. Yamada, & K. Aoki (San Francisco, CA: ASP), 298
Lotz, J. M., Jonsson, P., Cox, T. J., & Primack, J. R. 2008a, MNRAS, 391, 1137
Lotz, J. M., et al. 2008b, ApJ, 672, 177
Marchesini, D., et al. 2007, ApJ, 656, 42
Marín, F. A., Wechsler, R. H., Frieman, J. A., & Nichol, R. C. 2008, ApJ, 672, 849
McIntosh, D. H., Guo, Y., Hertzberg, J., Katz, N., Mo, H. J., van den Bosch, F. C., & Yang, X. 2008, MNRAS, 388, 1537
Melbourne, J., et al. 2005, ApJ, 625, L27
Melbourne, J., et al. 2008, AJ, 135, 1207
Mihos, J. C., & Hernquist, L. 1996, ApJ, 464, 641
Neistein, E., & Dekel, A. 2008, MNRAS, 388, 1792
Noeske, K. G., et al. 2007, ApJ, 660, L47
Patton, D. R., & Atfield, J. E. 2008, ApJ, 685, 235
Patton, D. R., et al. 2002, ApJ, 565, 208
Peebles, P. J. E. 1982, ApJ, 263, L1
Purcell, C. W., Bullock, J. S., & Zentner, A. R. 2007, ApJ, 666, 20
Purcell, C. W., Kazantzidis, S., & Bullock, J. S. 2009, ApJ, 694, L98
Quadri, R., et al. 2007, AJ, 134, 1103
Robertson, B. E., & Bullock, J. S. 2008, ApJ, 685, L27
Robertson, B., Bullock, J. S., Cox, T. J., Di Matteo, T., Hernquist, L., Springel, V., & Yoshida, N. 2006a, ApJ, 645, 986
Robertson, B., Cox, T. J., Hernquist, L., Franx, M., Hopkins, P. F., Martini, P., & Springel, V. 2006b, ApJ, 641, 21
Rocha, M., Jonsson, P., Primack, J. R., & Cox, T. J. 2008, MNRAS, 383, 1281
Ryan, Jr., R. E., Cohen, S. H., Windhorst, R. A., & Silk, J. 2008, ApJ, 678, 751
Sawicki, M., & Thompson, D. 2006, ApJ, 642, 653
Shapley, A. E., Steidel, C. C., Adelberger, K. L., Dickinson, M., Giavalisco, M., & Pettini, M. 2001, ApJ, 562, 95
Shapiro, K. L., et al. 2008, ApJ, 682, 231
Somerville, R. S., Hopkins, P. F., Cox, T. J., Robertson, B. E., & Hernquist, L. 2008, MNRAS, 391, 481
Springel, V., Di Matteo, T., & Hernquist, L. 2005, MNRAS, 361, 776
Springel, V., & Hernquist, L. 2003, MNRAS, 339, 289
Springel, V., et al. 2005, Nature, 435, 629
Stewart, K. R. 2009, in Proceedings of Galaxy Evolution: Emerging Insights and Future Challenges, in press (arXiv:0902.2214)
Stewart, K. R., Bullock, J. S., Wechsler, R. H., & Maller, A. H. 2009, ApJ, submitted (arXiv:0901.4336)
Stewart, K. R., Bullock, J. S., Wechsler, R. H., Maller, A. H., & Zentner, A. R. 2008, ApJ, 683, 597
Tasitsiomi, A., Kravtsov, A. V., Wechsler, R. H., & Primack, J. R. 2004, ApJ, 614, 533
Toomre, A., & Toomre, J. 1972, ApJ, 178, 623
Vale, A., & Ostriker, J. P. 2004, MNRAS, 353, 189
Villalobos, Á., & Helmi, A. 2008, MNRAS, 391, 1806
Wechsler, R. H., Bullock, J. S., Primack, J. R., Kravtsov, A. V., & Dekel, A. 2002, ApJ, 568, 52
Wechsler, R. H., Zentner, A. R., Bullock, J. S., Kravtsov, A. V., & Allgood, B. 2006, ApJ, 652, 71
Wetzel, A. R., Cohn, J. D., & White, M. 2009, MNRAS, 395, 1376
Wolf, C., et al. 2005, ApJ, 630, 771
Wright, S. A., Larkin, J. E., Law, D. R., Steidel, C. C., Shapley, A. E., & Erb, D. K. 2009, ApJ, 699, 421
Yepes, G., Kates, R., Khokhlov, A., & Klypin, A. 1997, MNRAS, 284, 235
Younger, J. D., Cox, T. J., Seth, A. C., & Hernquist, L. 2007, ApJ, 670, 269